Environmental Research Letters

LETTER

Identifying the complex types of atmosphere-ocean interactions in El Niño

Wan-Jiao Song[1,2,3] and Jin-Yi Yu[2,3]

1   National Satellite Meteorological Center, China Meteorological Administration, Beijing, People's Republic of China
2   Department of Earth System Science, University of California, Irvine, California, United States of America
3   Authors to whom any correspondence should be addressed.

E-mail: songwj@cma.gov.cn and jyyu@uci.edu

Abstract

A technique is developed to identify the types of atmosphere-ocean interaction during El Niño-Southern Oscillation events using sea surface temperature, sea level pressure (SLP), and outgoing longwave radiation (OLR) data. Two pairs of indices are derived that separate the interactions into tropical and subtropical types and basin-wide and local types. The dominant interaction type for the observed El Niño events since 1980 is identified and shown to shift with time from the tropical to subtropical and from basin-wide to local. Thus, the 21st century El Niños have become dominated by subtropical and local interactions, in strong contrast to the 20th century El Niños that were dominated by the tropical and basin-wide interactions. These changes result in the 1997–98 and 2015–16 extreme El Niños being different in their evolutions and global impacts, despite having similar intensities. SLP is the key variable for separating the tropical and subtropical types of interactions, while OLR is the key variable for separating the basin-wide and local types of interactions.

1. Introduction

El Niño-Southern Oscillation (ENSO) is an important climate variation phenomenon that arises from interactions between the tropical Pacific Ocean and the overlying atmosphere (Bjerknes 1969, Rasmusson and Carpenter 1982, Philander 1990, Latif *et al* 1994). There have been continuous efforts in the research community to develop indices that can better characterize and quantify this important climate phenomenon. Warming of sea surface temperatures (SSTs) in the tropical Pacific Ocean is the most obvious feature that characterizes the ENSO and, therefore, SSTs have been frequently used to construct ENSO indices. The Ocean Niño Index (ONI), for example, is one of the most popular indices that the community uses to monitor the intensity of ENSO events. Recent studies have demonstrated that more than one type of ENSO exists: the conventional Eastern Pacific (EP) type and the increasingly occurring Central Pacific (CP) type (Yu and Kao 2007, Kao and Yu 2009). The CP ENSO is

also referred to as the Dateline El Niño (Larkin and Harrison 2005), El Niño Modoki (Ashok *et al* 2007), or warm pool El Niño (Kug *et al* 2009). This complexity in ENSO type suggests that more than a single index is required to describe ENSO characteristics.

The new indices that have been developed so far are mostly still SST-based. Empirical Orthogonal Function (EOF) analysis is one of the most popular statistical methods used to construct the indices, as it has the ability to identify distinct variability modes. For example, the El Niño Modoki index constructed by Ashok *et al* (2007) and the EP and CP Indices constructed by Kao and Yu (2009) both used this property of EOF analysis to separate the EP and CP types of ENSO. Takahashi *et al* (2011) showed that indices constructed by rotating the principal components (PCs) of the first two leading modes of the EOF analysis result in indices that can adequately represent the variability associated with EP and CP El Niño events. We notice that the E-index and C-index produced by this PC-rotation method are highly correlated with the EP

index and CP index produced by the EOF-regression method of Kao and Yu (2009). Therefore, the PC-rotation method appears to be an effective and simple way to construct pairs of indices to monitor different characteristics of ENSO.

While SST-based indices can represent the strength of ocean warming during ENSO events, they do not reflect another key characteristic of ENSO, which is the interaction between the tropical Pacific Ocean and the overlying atmosphere. Atmospheric information must be added to the SST information to construct indices that can reveal the interaction characteristics of El Niño. The Multivariate ENSO Index (MEI; Wolter and Timlin 1993, 2011) is one example of such an index. It uses a total of six atmospheric and oceanic variables. However, different types of ENSO may involve different interaction processes (e.g. Yu *et al* 2010, Yu and Kim 2011) and thus more than one single interaction index is required to account for the complex ENSO interaction characteristics. In this study, we develop pairs of multivariable indices using a PC-rotation method and use the pair indices to identify different interaction characteristics of El Niño events. Different from the way the MEI index was constructed, we add atmospheric variables one by one to SST to examine their different abilities of revealing the characteristics of atmosphere-ocean interactions during ENSO. We choose to consider two key atmospheric variables for the interactions: one is sea level pressure (SLP) and the other is outgoing longwave radiation (OLR). The former responds to the heating from ENSO and in turn drives winds to force the ocean, while the latter responds to atmospheric heating during ENSO and provides a key connection among SST, wind, and SLP anomalies (Chiodi and Harrison 2013).

2. Data and methods

Several monthly-mean datasets were used in this study, these include SST from National Oceanic and Atmospheric Administration (NOAA) Extended Reanalysis SST V2.0 (Reynolds *et al* 2002), OLR from NOAA Interpolated Outgoing longwave Radiation (Liebmann and Smith 1996), and SLP from the National Centers for Environmental Prediction-National Centre for Atmospheric Research Reanalysis (Kalnay *et al* 1996). All the datasets were re-gridded to a uniform spatial resolution ($2.5° \times 2.5°$) for this analysis. The analysis period is from January 1980 to December 2017 and the analysis domain focuses on the Tropical Pacific Ocean between 90 °E-90°W and 30 °S-30°N. The seasonal cycle for each variable is calculated with reference to the period 1980–2017. Anomalies are defined as the deviations from the seasonal cycle after the linear trend is removed. Also used in the analysis is the time series of monthly ONI values, which are defined as the SST anomalies

averaged within the Niño3.4 region (5 °S-5°N; 170 °W-120°W).

We adapt the PC-rotation method of Takahashi *et al* (2011) to construct multivariate ENSO InTeraction (EIT) indices using the following procedure. We first apply a multivariate EOF (MEOF) analysis to the combined SST and SLP anomalies or combined SST and OLR anomalies in the tropical Pacific domain. The EOF was applied to the correlation matrix of the variables to ensure that the EOF loadings are not affected by the different units or variance magnitudes. We consider these two EOF modes to be dynamically different. Their spatial patterns do not need to be orthogonal to each other. The different 'dynamics' that these EOF modes represent are the different 'interaction dynamics' of ENSO. The dynamical differences are supported by the physical processes that we present based on the spatial patterns of the two variables (e.g. SST and SLP or SST and OLR). The PCs of the first two leading MEOF modes (i.e. PC1 and PC2) are then added and subtracted following equations (1) and (2) to produce a pair of indices, which we refer to as the EIT1 and EIT2 indices:

$$EIT1 = (PC1 - PC2)/\sqrt{2}, \qquad (1)$$

$$EIT2 = (PC1 + PC2)/\sqrt{2}. \qquad (2)$$

3. Results

We first used the PC-rotation method to construct the interaction indices using the combined SST and SLP anomalies. We refer to these two indices as $EIT1_{slp}$ and $EIT2_{slp}$ hereafter. We examine the characteristics of ENSO interaction associated with these two indices by regressing anomalies onto the indices. The regressed SST anomaly structures (figures 1(a) and (c)) indicate that the $EIT1_{slp}$ is characterized by SST anomalies centered in the tropical eastern Pacific that resemble those associated with the EP ENSO, whereas the $EIT2_{slp}$ is characterized by anomalies centered in the tropical central Pacific that resemble those associated with the CP ENSO. The regressed SLP anomalies associated with the $EIT1_{slp}$ Index resemble the Southern Oscillation pattern characterized by an east–west seesaw of SLP anomalies within the tropical Pacific (figure 1(b)), while the anomalies associated with the $EIT2_{slp}$ index are characterized by out-of-phase SLP anomalies between the Maritime Continent and the subtropics of both the North and South Pacific (figure 1(d)). Figures 1(a)–(d) indicate that the $EIT1_{slp}$ index is related to the interaction between ENSO SST variations and tropical SLP variations, and that the $EIT1_{slp}$ index is related to the interaction between ENSO SST variations and subtropical SLP variations. Therefore, the former index can be used to quantify the tropical interaction of ENSO whereas the latter can quantify the subtropical interaction of ENSO.
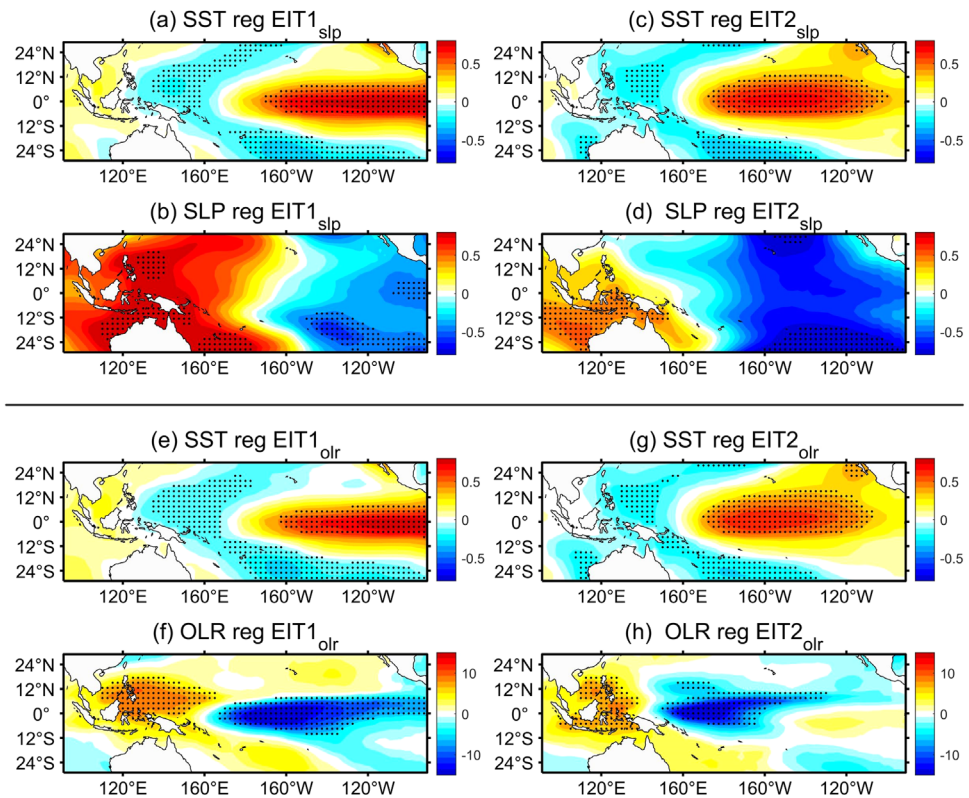
Figure 1. SST (a), (c) and SLP (b), (d) anomalies associated with the EIT1$_{slp}$ and EIT2$_{slp}$ indices. SST (e), (g) and OLR (f), (h) anomalies associated with the EIT1$_{olr}$ and EIT2$_{olr}$ indices. Values shown are the linear regression coefficients of the anomalies onto the indices. Units are °C for SST, millibar for SLP and W m-2 for OLR. Black dots mark regions where the regression coefficients are significant at the 90% confidence level based on a Student's *t*-test.
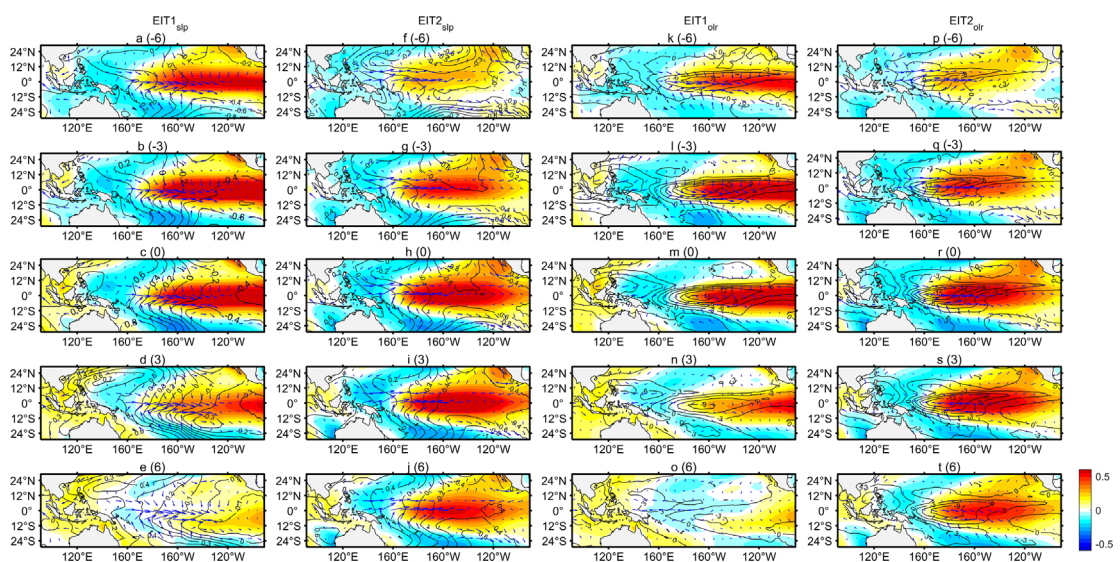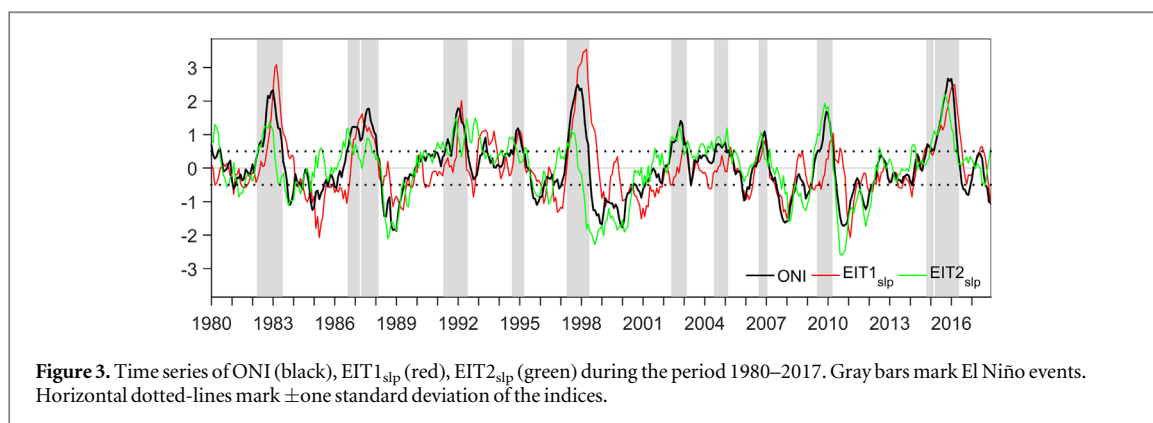

Figure 2. Lead-lagged regressions of SST (color), SLP (contour) and wind (vector) anomalies onto the EIT1$_{slp}$ (a)–(e) and EIT2$_{slp}$ (f)–(j) indices. Lead-lagged regressions of SST (color), OLR (contour) and wind (vector) anomalies onto the EIT1$_{olr}$ (k)–(o) and EIT2$_{olr}$ (p)–(t) indices. The lag values (months) are shown at the top of each panel. Units are °C for SST, millibar for SLP and W m-2 for OLR.

To further examine the ocean-atmosphere interactions associated with the two indices, we show in figure 2 the lead-lagged regressions of SLP, SST, and surface wind anomalies onto EIT1$_{slp}$ and EIT2$_{slp}$. The regressions onto EIT1$_{slp}$ (figures 2(a)–(e)) reveal a tropical Pacific interaction that resembles the Bjerknes feedback mechanism (Bjerknes 1969). The east–west gradient of tropical Pacific SST anomalies drives changes in the zonal circulation of the tropical atmosphere (i.e. the Walker circulation), which are reflected in the large surface westerly anomalies over the tropical Pacific. The wind anomalies then influence the

Letters

Figure 3. Time series of ONI (black), EIT1$_{slp}$ (red), EIT2$_{slp}$ (green) during the period 1980–2017. Gray bars mark El Niño events. Horizontal dotted-lines mark $\pm$one standard deviation of the indices.

thermocline slope along the tropical Pacific (not shown) to intensify the east–west SST gradient via equatorial upwelling (e.g. Kim and Jin 2011). The regressions onto EIT2$_{slp}$ (figures 2(f)–(j)) show a subtropical Pacific interaction that resembles the seasonal footprint mechanism (Vimont *et al* 2003, Yu and Fang 2018). Previous studies (Yu *et al* 2010, Yu and Kim 2011, Yu *et al* 2017) have pointed out that the negative subtropical SLP anomaly pattern first produces anomalous surface southwesterly winds. The wind anomalies reduce surface latent heat fluxes to induce positive subtropical SST anomalies (figure 2(f)). The SST anomalies then perturb and maintain the SLP and wind anomalies. Through this wind-evaporation-SST feedback (Xie and Philander 1994), the subtropical SST anomalies can be maintained for a few seasons and at the same time spread equatorward into the tropical Pacific to become tropical SST anomalies (figures 2(g)–(h)). The anomalies later develop into an El Niño event in the tropical central Pacific (figures 2(h)–(j)).
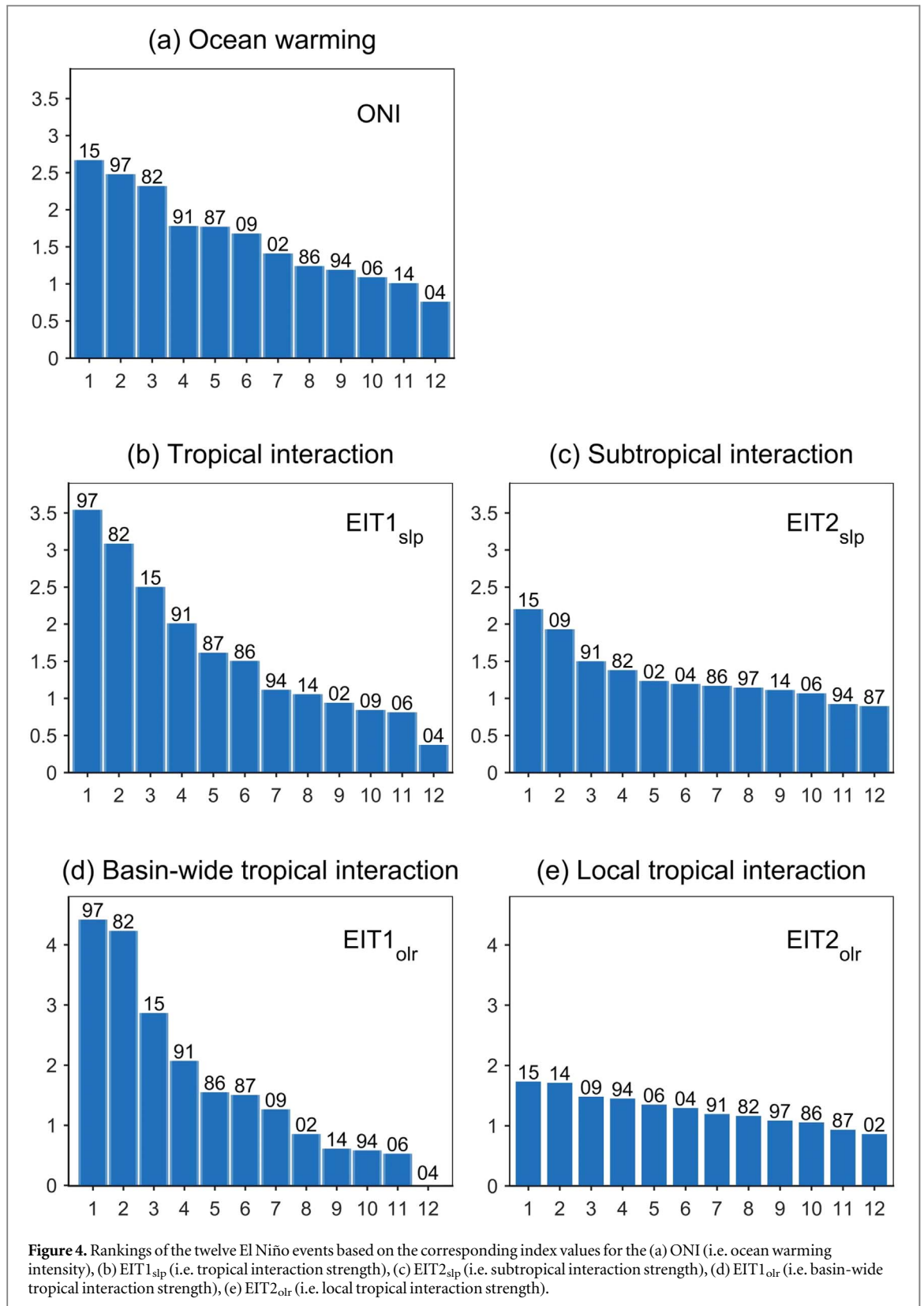
To examine the tropical and subtropical interaction strengths during ENSO events, we show in figure 3 the time series of the EIT1$_{slp}$ and EIT2$_{slp}$ indices with that of the ONI during the analysis period. Here the ONI is also used to identify the El Niño events following the NOAA Climate Prediction Center's criteria (see Text S1 is available online at stacks.iop.org/ERL/14/114030/mmedia). There are twelve El Niño events during the analysis period (listed in table S1 and indicated by gray shading in figure 3).

By monitoring the EIT1$_{slp}$ and EIT2$_{slp}$ indices, we can determine the relative contributions of tropical and subtropical interactions to each of the El Niño events. Based on the ONI values, the 2015–16, 1997–98, and 1982–83 events are the three strongest El Niño events and have similar intensities. However, the EIT1$_{slp}$ and EIT2$_{slp}$ indices reveal very different characteristics of ocean-atmosphere interaction behind these three events. The 1997–98 El Niño is dominated by the tropical interaction, as it has large EIT1$_{slp}$ values but small EIT2$_{slp}$ values. The 1982–83 El Niño is also a tropical interaction event of El Niño, but this event is influenced more by the subtropical interaction during

the early stages of the event than the 1997–98 El Niño. As for the 2015–16 El Niño, it is dominated by both the tropical and subtropical interactions with comparable strengths. This is consistent with the suggestion of Paek *et al* (2017) that the stronger subtropical Pacific influence caused the 2015–16 El Niño to evolve differently from the 1997–98 El Niño and produced different remote climate impacts.

In figure 4, we rank the intensities of the twelve El Niño events according to the maximum values of the ONI, EIT1$_{slp}$ and EIT2$_{slp}$ indices during events. In terms of the magnitude of ocean warming, the six strongest El Niños are the 2015–16, 1997–98, 1982–83, 1991–92, 1987–88, and 2009–10 events (figure 4(a)). It is interesting to note that rankings obtained with the ONI are very different from those obtained using the EIT1$_{slp}$, which implies that the conventional ENSO interaction mechanism (i.e. the tropical interaction process/Bjerknes feedback mechanism) alone cannot account for ENSO intensity. Other interaction processes need to be considered. We also notice that five out of the six strongest tropical interaction events of El Niño (1997–98, 1982–83, 2015–16, 1991–92, 1987–88, 1986–87) occurred in the 20th century (figure 4(b)), while four out of the six strongest subtropical interaction events of El Niño (2015–16, 2009–10, 1991–92, 1982–83, 2002–03, and 2004–05) occurred in the 21st century (figure 4(c)). There is a tendency for El Niño to shift from being dominated by the tropical interaction in the 20th century to being dominated by the subtropical interaction in the 21st century.
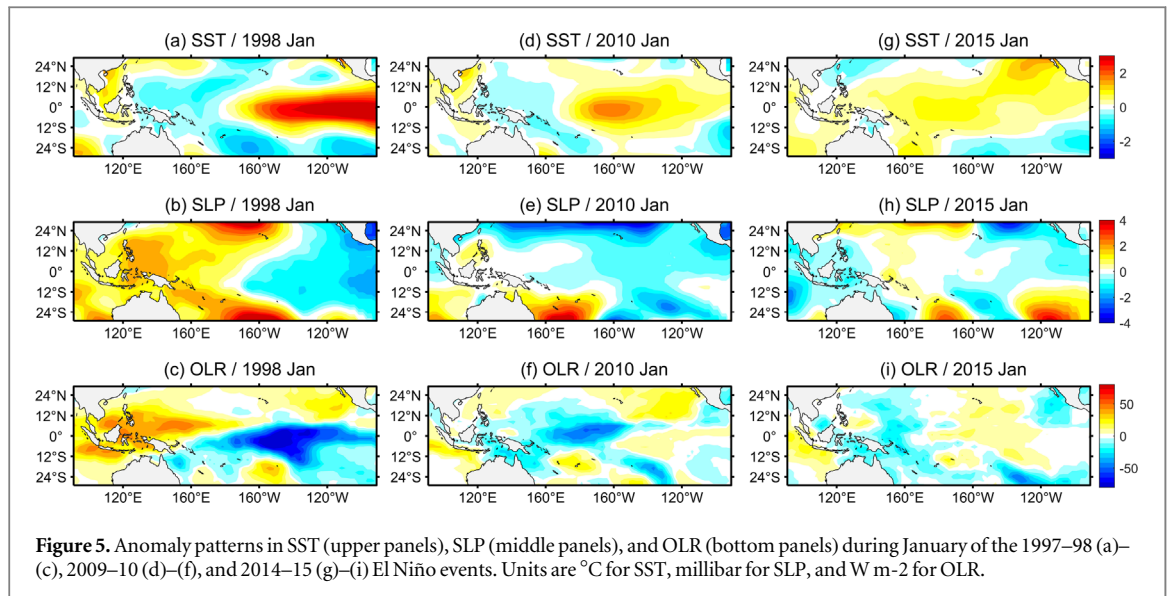
Next, we examine interaction indices using OLR instead of SLP. We applied the PC-rotation method again but with the MEOF analysis using combined SST and OLR anomalies. This pair of interaction indices are referred to as the EIT1$_{olr}$ and EIT2$_{olr}$ indices. The anomaly structures associated with these two indices are shown in figures 1(e)–(h), where SST and OLR anomalies are regressed onto the indices. The regressed SST anomalies associated with the EIT1$_{olr}$ and EIT2$_{olr}$ indices (figures 1(e) and (g)) resemble respectively the EP and CP ENSOs, and are similar to those associated with the EIT1$_{slp}$ and EIT2$_{slp}$ indices. The

Figure 4. Rankings of the twelve El Niño events based on the corresponding index values for the (a) ONI (i.e. ocean warming intensity), (b) $EIT1_{slp}$ (i.e. tropical interaction strength), (c) $EIT2_{slp}$ (i.e. subtropical interaction strength), (d) $EIT1_{olr}$ (i.e. basin-wide tropical interaction strength), (e) $EIT2_{olr}$ (i.e. local tropical interaction strength).

regressed OLR anomalies associated with the $EIT1_{olr}$ index (figure 1(f)) are characterized by suppressed convection (i.e. positive anomalies) over the tropical western Pacific and a long strip of enhanced convection (i.e. negative anomalies) over the equatorial central-to-eastern Pacific. In contrast, the negative OLR anomalies associated with the $EIT1_{olr}$ index have a

narrower longitudinal extension (figure 1(h)) in the equatorial Pacific. Therefore, the interaction index pair constructed from combined SST and OLR anomalies represent the basin-wide and local types of tropical interaction during ENSO, respectively.

To further examine the ocean-atmosphere interactions associated with these two OLR indices, we

Figure 5. Anomaly patterns in SST (upper panels), SLP (middle panels), and OLR (bottom panels) during January of the 1997–98 (a)–(c), 2009–10 (d)–(f), and 2014–15 (g)–(i) El Niño events. Units are °C for SST, millibar for SLP, and W m-2 for OLR.

show in figures 2(k)–(t) the lead-lagged regressions of OLR, SST, and surface wind anomalies onto $EIT1_{olr}$ and $EIT2_{olr}$. The regressions onto $EIT1_{olr}$ (figures 2(k)–(o)) indicate that the SST anomalies in the tropical eastern Pacific perturb the Walker circulation (which is evident by the surface westerly anomalies across most of the tropical Pacific). The perturbed Walker circulation results in basin-wide convection variations, which are manifested as a long strip of OLR anomalies in the tropical central-to-eastern Pacific. The anomalous convection result in heating anomalies that further perturb the Walker circulation (and the surface wind anomalies). The regressions onto $EIT2_{olr}$ (figures 2(p)–(t)) indicate that SST anomalies in the tropical central Pacific are less capable of perturbing the Walker circulation (Zou *et al* 2014), which is evident by the lack of basin-wide surface westerly anomalies. Westerly anomalies were confined to a narrower strip to the west of the SST anomalies. The narrow wind anomalies are located near where the narrow OLR anomalies are located, which indicates a local interaction. Therefore, the $EIT1_{olr}$ and $EIT2_{olr}$ index respectively reveal the basin-wide and local thermodynamic interaction between the ocean and the atmosphere through OLR heating. Our analyses find SLP to be useful in separating the tropical and subtropical interactions during ENSO, and OLR to be useful in separating the basin-wide and local types of tropical interaction.

We ranked the twelve El Niño events according to the values of their $EIT1_{olr}$ and $EIT2_{olr}$ indices (figures 4(d) and (e)) and find that five out of the six strongest basin-wide interaction events (1997–98, 1982–83, 2015–16, 1991–92, 1986–87, 1987–88) occurred in the 20th century and five out of the six strongest local interaction El Niño events (2015–16, 2014–15, 2009–10, 1994–95, 2006–07, 2004–05) occurred in the 21st century. It seems that the tropical interaction during ENSO events has changed from the

basin-wide type to the local type in recent decades. It is particularly interesting to note that the 2014–15 El Niño was ranked #2 in local interaction strength, although it ranked #11 in terms of the strength of SST warming (see figure 4(a)). This event was considered by some studies as a 'failed' or 'borderline' El Niño that did not develop to the expected strength based on the anomalous ocean heat content observed. It has been argued that this failure was due to the weak atmosphere-ocean interaction during the event, which may be a result of the interruption caused by easterly wind bursts along the equator (e.g. Menkes *et al* 2014, Hu and Fedorov 2016). Our analysis indicates that the very strong local interaction (rather than basin-wide interaction) can be another explanation for why this event did not fully develop. It is noticed that the basin-wide interaction tends to produce stronger El Niño events than the local interaction does. This is likely due to the fact that the basin-wide interaction can perturb the Walker circulation to produce stronger Bjerknes feedback than the local interaction.

Based on the ranking in figure 4, we performed case studies for 1997–98, 2009–10, and 2014–15 El Niños to examine if the complex interaction characteristics revealed by the two pairs of the EIT indices can be verified. SST, SLP, and OLR anomalies of these events during January (which is typically the time of the peak phase of ENSO) are shown in figure 5. The 1997–98 El Niño is used to examine the tropical interaction characteristics, because this event has the strongest tropical interaction but weak subtropical interaction (ranked #8). As expected from the interaction characteristics revealed by the EIT indices, this event is characterized by SST anomalies centered in the tropical eastern Pacific (figure 5(a)) that are associated with a Southern Oscillation pattern of SLP anomalies (figure 5(b)), and this tropical interaction is of a basin-wide nature that is manifested by a long strip of negative OLR anomalies along the equatorial

Pacific (figure 5(c)). We choose the 2009–10 El Niño to examine the subtropical interaction characteristics, as it has the second strongest subtropical interaction but weak tropical interaction (ranked #10). The strongest subtropical interaction event is the 2015–16 El Niño, but this event also has very strong tropical interaction (ranked #3), so it is not the best case to use to isolate the subtropical interaction characteristics. The 2009–10 El Niño is characterized by SST anomalies centered in the tropical central Pacific (figure 5(d)) that are associated with large SLP anomalies over the northern and southern subtropical Pacific (figure 5(e)) and is associated with OLR anomalies in equatorial central Pacific (rather than in the equatorial central-to-eastern Pacific as in the 1997–98 El Niño). These features are consistent with what the EIT2$_{slp}$ and EIT2$_{olr}$ indices reveal. The 2014–15 El Niño is used to verify the characteristics of the local type of tropical interaction, as it has the second strongest local tropical interaction but weak basin-wide tropical interaction (ranked #9). Figures 5(g)–(i) show that the 2014–15 event has weak SST anomalies in the tropical central Pacific and in the area of the Pacific Meridional Mode (Chiang and Vimont 2004), large SLP anomalies over the northern and southern subtropical Pacific, and an extremely weak band of negative OLR anomalies to the west of the International Dateline. The negative OLR anomalies in this event occupy a much narrower band than those in the 2009–10 El Niño. These three case studies confirm that the multivariable interaction indices developed here with SST, SLP, and OLR are effective in quantifying the strengths of the complex interaction characteristics during ENSO.

4. Conclusion and discussion

Using a PC-rotation method and a MEOF analysis, we developed two pairs of ENSO interaction indices using SST, SLP, and OLR anomalies to examine the complex characteristics of ENSO. The indices indicate that the ocean-atmosphere interaction crucial to ENSO can be classified into at least four different types: tropical interaction, subtropical interaction, basin-wide tropical interaction, and local tropical interaction. More than one interaction type can be associated with a given ENSO event. The newly developed interaction indices can be used to quantify the strengths of each of these four types of interaction, enabling us to determine which interaction processes are involved and most important for each ENSO event. The usefulness of the indices was demonstrated by examining them during the twelve El Niño events that occurred during 1980–2017. The analysis reveals the 1997–98 and 2015–16 extreme El Niños were dominated by different interaction processes, despite the fact that they have similar intensities of ocean warming. The 1997–98 El Niño is almost completely dominated by tropical interaction, but the 2015–16 El Niño involved

both tropical and subtropical interactions. Therefore, the PC-rotation method appears to be an effective and simple way to construct pairs of indices to monitor the complex interactions during ENSO although it can be limited by the selections of the analysis area and period. This study also finds that El Niño has changed in recent decades from being dominated by the tropical interaction to being dominated by the subtropical interaction and from being dominated by the basin-wide interaction to being dominated by the local interaction. The findings from this study offer a new way to understand and study the ENSO complex ocean-atmosphere interactions driving ENSO.

It should be pointed out that our indices identify the large spatial scale and interannual time scale interactions associated with ENSO. State-dependent or random noise (such as those associated with intraseasonal variability, stochastic forcing from the atmosphere, etc) are also important factors for ENSO interactions (Hu *et al* 2004, Kug *et al* 2008, Philip and Oldenborgh 2010, Levine *et al* 2017), but their contributions are not included in the indices we defined in this study. In this study, we only used SST, SLP, and OLR to derive ocean-atmosphere interaction indices. One reason for the choice is that all three variables tend to vary in space more slowly and are less noisy than other variables (such as wind and precipitation). They are more likely to result in distinguishable modes in the MEOF analysis.

Data availability statement

The SST data of Extended Reconstructed Sea Surface Temperature, monthly SLP and OLR fields of National Centers for Environmental Prediction/National Center for Atmospheric Research (NCEP–NCAR) were obtained from NOAA (https://www.esrl.noaa.gov/psd/), the ONI index was also downloaded from NOAA (https://origin.cpc.ncep.ncep.gov/products/analysis_monitoring/ensostuff/ONI_v5.php/). Any other data that support the findings of this study are included within the article.

ORCID iDs

Wan-Jiao Song ⬡ https://orcid.org/0000-0003-3236-5824
Jin-Yi Yu ⬡ https://orcid.org/0000-0001-6156-7623

References

Ashok K, Behera S K, Rao S A, Weng H Y and Yamagata T 2007 El Niño Modoki and its possible teleconnection *J. Geophys. Res.* **112** C11007

Bjerknes J. 1969 Atmospheric teleconnections from the equatorial Pacific *Mon. Weather Rev.* **97** 163–72

Chiang J C H. and Vimont D J 2004 Analogous Pacific and Atlantic meridional modes of tropical atmosphere–ocean variability *J. Clim.* **17** 4143–58

Chiodi A M and Harrison D E 2013 El Niño impacts on seasonal US atmospheric circulation, temperature, and precipitation anomalies: the OLR-event perspective *J. Clim.* **26** 822–37

Hu S N and Fedorov A V 2016 Exceptionally strong easterly wind burst stalling El Niño of 2014 *Proc. Natl Acad. Sci.* **113** 2005–10

Hu Z, Schneider E K, Bhatt U S and Kirtman B P 2004 Potential mechanism for response of El Niño-Southern Oscillation variability to change in land surface energy budget *J. Geophys. Research: Atmos.* **109** D21113

Kalnay E *et al* 1996 The NCEP/NCAR 40-Year Reanalysis Project *Bull. Am. Meteorol. Soc.* **77** 437–71

Kao H Y and Yu J Y 2009 Contrasting eastern-Pacific and central-Pacific types of ENSO *J. Clim.* **22** 615–32

Kim S T and Jin F F 2011 An ENSO stability analysis:I. Results from a hybrid coupled model *Clim. Dyn.* **36** 1593–607

Kug J, Jin F F, Sooraj K P and Kang I 2008 State-dependent atmospheric noise associated with ENSO *Geophys. Res. Lett.* **35** L05701

Kug J, Jin F F and An S 2009 Two types of El Niño events: cold tongue El Niño and warm pool El Niño *J. Clim.* **22** 1499–515

Larkin N K and Harrison D E 2005 Global seasonal temperature and precipitation anomalies during El Niño autumn and winter *Geophys. Res. Lett.* **32** L16705

Latif M, Barnett T P, Cane M A, Flügel M, Graham N E, Storch V H, Xu J S and Zebiak S E 1994 A review of ENSO prediction studies *Clim. Dyn.* **9** 167–79

Levine A F Z, Jin F F and Stuecker M F 2017 A simple approach to quantifying the noise–ENSO interaction:II. The role of coupling between the warm pool and equatorial zonal wind anomalies *Clim. Dyn.* **48** 19–37

Liebmann B and Smith C A 1996 Description of a complete (Interpolated) outgoing longwave radiation dataset *Bull. Am. Meteorol. Soc.* **77** 1275–7

Menkes C E, Lengaigne M, Vialard J, Puy M, Marchesiello P, Cravatte S and Cambon G 2014 About the role of Westerly Wind Events in the possible development of an El Niño in 2014 *Geophys. Res. Lett.* **41** 6476–83

Paek H, Yu J Y and Qian C C 2017 Why were the 2015/2016 and 1997/1998 extreme El Niños different? *Geophys. Res. Lett.* **44** 1848–56

Philander S G 1990 *El Niño, La Niña, and the Southern Oscillation* (*International Geophysics Series*) ed C Wunsch vol 46 (San Diego, CA: Academic) p 289

Philip S Y and Oldenborgh G J 2010 Atmospheric properties of ENSO: models versus observations *Clim. Dyn.* **34** 1073–91

Rasmusson E M and Carpenter T H 1982 Variations in tropical sea surface temperature and surface wind fields associated with the Southern Oscillation/El Niño *Mon. Weather Rev.* **110** 354–84

Reynolds R W, Rayner N A, Smith T M, Stokes D C and Wang W 2002 An Improved *in situ* and satellite SST analysis for climate *J. Clim.* **15** 1609–25

Takahashi K, Montecinos A, Goubanova K and Dewitte B 2011 ENSO regimes: reinterpreting the canonical and Modoki El Niño *Geophys. Res. Lett.* **38** L10704

Vimont D J, Wallace J W and Battisti D S 2003 The seasonal footprinting mechanism in the pacific: implications for ENSO *J. Clim.* **16** 2668–75

Wolter K and Timlin M S 1993 Monitoring ENSO in COADS with a seasonally adjusted principal component index *Proc. 17th Climate Diagnostics Workshop* pp 52–7 Norman, OK, NOAA/NMC/CAC, NSSL, Oklahoma Climatological Survey, CIMMS and the School of Meteor., University of Oklahoma

Wolter K and Timlin M S 2011 El Niño/Southern oscillation behaviour since 1871 as diagnosed in an extended multivariate ENSO index (MEI.ext) *Int. J. Climatol.* **31** 1074–87

Xie S P and Philander S G H 1994 A coupled ocean-atmosphere model of relevance to the ITCZ in the eastern Pacific *Tellus* A **46** 340–50

Yu J Y and Fang S W 2018 The distinct contributions of the seasonal footprinting and charged–discharged mechanisms to ENSO complexity *Geophys. Res. Lett.* **45** 6611–8

Yu J Y, Kao H Y and Lee T 2010 Subtropics-related interannual sea surface temperature variability in the central equatorial Pacific *J. Clim.* **23** 2869–84

Yu J Y and Kim S T 2011 Relationships between extratropical sea level pressure variations and the central Pacific and Eastern Pacific types of ENSO *J. Clim.* **24** 708–20

Yu J Y and Kao H Y 2007 Decadal changes of ENSO persistence barrier in SST and ocean heat content indices: 1958-2001 *J. Geophys. Res.* **112** D12106

Yu J Y, Wang X, Yang S, Paek H and Chen M 2017 Changing El Niño–Southern Oscillation and associated climate extremes *Climate Extremes: Patterns and Mechanisms* (*Geophysical Monograph Series*) ed S Y Wang, J H Yoon, C Funk and R R Gillies (Washington, DC: American Geophysical Union)

Zou Y H, Yu J Y, Lee T, Lu M M and Kim S T 2014 CMIP5 model simulations of the impacts of the two types of El Niño on the US winter temperature *J. Geophys. Res.: Atmos.* **119** 3076–92

1
2
3   *Environmental Research Letters*
4
5   Supporting Information for
6
7
8
9
10

11   **Identifying the complex types of atmosphere-ocean interactions in El**
12   **Niño**

13   Wan-Jiao Song[1,2] and Jin-Yi Yu[2]

14

15   1.   National Satellite Meteorological Center,
16   China Meteorological Administration, Beijing, China
17
18   2.Department of Earth System Science,
19   University of California, Irvine, California, USA
20
21
22
23
24
25   **Contents of this file**

26   Text S1

27   Figure S1

28   Table S1

29

Text S1. Methods used to identify El Niño events

The Ocean El Niño Index (ONI) is used to identify El Niño events, and is defined as the ERSST.v5 SST averaged in the Niño3.4 region (5°N-5°S, 120°-170°W). An El Niño event is identified when the 3-month running ONI value exceeds a threshold of +0.5℃ (-0.5℃) for more than 5 consecutive months (Figure S1). Based on these criteria, a total of twelve El Niño events (1982, 1986, 1987, 1991, 1994, 1997, 2002, 2004, 2006, 2009, 2014, 2015) occurred during the analysis period. The starting and ending time of each of the twelve events are listed in Table S1.
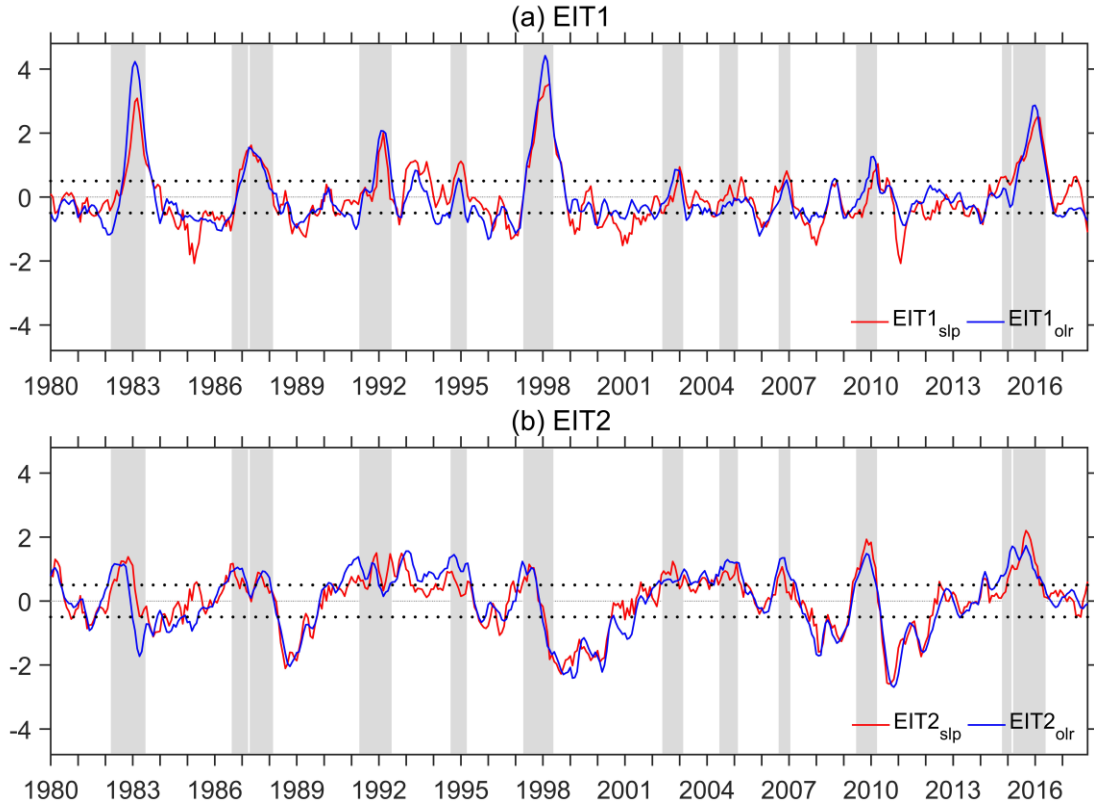
Fig. S1: Time series of EIT1 (a) and EIT2 (b) obtained by separately applying Multivariable Empirical Orthogonal Function (MEOF) analysis to combined sea surface temperature (SST) and sea level pressure (SLP) anomalies and combined SST and outgoing longwave radiation (OLR) anomalies during 1980-2017. The EIT indices obtained from the combined SST and SLP anomalies are shown in red, while the indices obtained from the combined SST and OLR anomalies are shown in blue. Gray bars mark El Niño events. Horizontal dotted-lines mark ±one standard deviation of the indices.

48 **Tab. S1:** Durations of the twelve El Niño events during 1980-2017

Event	Duration
1982-83	April 1982 – June 1983
1986-87	September1986 – April 1987
1987-88	May 1987 - February 1988
1991-92	May 1991- June 1992
1994-95	September 1994 – March 1995
1997-98	May 1997 – May 1998
2002-03	June 2002 – February 2003
2004-05	July 2004 – February 2005
2006-07	September 2006 – January 2007
2009-10	July 2009 – March 2010
2014-15	November 2014 – March 2015
2015-16	April 2015 – May 2016

49